Fire weather climatology dataset for Victoria Supplemental Report for Dataset Version 2

Supplemental Report to the Victoria Department of Environment, Land and Water Planning
June 2016
(Appendix A revision August 2016)

Timothy Brown[a,b], Graham Mills[b], Sarah Harris[b], Domagoj Podnar[a], Hauss Reinbold[a] and Matt Fearon[a]

[a]*Desert Research Institute, Reno Nevada USA, tim.brown@dri.edu*
[b]Monash University, Clayton Victoria Australia, sarah.harris@monash.edu

EXECUTIVE SUMMARY

Since the release of the original dataset, extensive work and evaluation was undertaken to improve the distributions for surface temperature, relative humidity and wind speed. Emphasis was given to improving the bias correction of the distribution tails. Quantile mapping was still used for this version, except that empirical cumulative distribution functions were employed rather than theoretical distributions. This allowed for better direct quantile matching between observations and model. Stricter quality control procedures were used on the observational data to remove additional erroneous values discovered after further testing.

Specific methodology modifications were undertaken that provided substantial improvements to the dataset. First, a careful QC of the observation dataset was required to remove unrealistic or unlikely values, since these would heavily influence the empirical distribution tails. Second, it was necessary to make sure that observation locations were not related to model water grid points since these would bias the correction. Third, because of diurnal, seasonal, and local physical characteristics of the observation stations (e.g., terrain), it was important to develop mapping functions for each hour by month. Fourth, much emphasis in assessing the correction was given the distribution tails, since this region is quite important for bushfire analyses. Fifth, the spatial interpolation of correction across the grid required a balance of weighting the station grid point to account for local characteristics and its influence on neighbouring stations.

This supplemental report describes the methods used to generate Version 2 of the Fire weather climatology dataset for Victoria. Version 2 replaces Version 1, and users should only work with this new version of the dataset given the substantial improvements that were made, particularly in the reduction of bias at the highest wind speeds and lowest relative humidity extremes of their distributions, and consequently substantially higher extreme values of the Forest Fire Danger Index (FFDI).

TABLE OF CONTENTS

1 BACKGROUND

Climatology data of fire weather across the landscape can provide science-based evidence for informing strategic decisions to ameliorate the impacts (at times extreme) of bushfires on community socio-economic wellbeing and to sustain ecosystem health and functions. A long-term climatology requires spatial and temporal data that are consistent to represent the landscape in sufficient detail to be useful for fire weather studies and management purposes. To address this inhomogeneity problem for analyses of a variety of fire weather interests and to provide a dataset for management decision-support, a homogeneous 41-year (1972-2012), hourly interval, 4 km gridded climate dataset for Victoria has been generated using a combination of mesoscale modelling, global reanalysis data, surface observations, and historic observed rainfall analyses. Hourly near-surface forecast fields were combined with Drought Factor (DF) fields calculated from the Australian Water Availability Project (AWAP) rainfall analyses to generate fields of hourly fire danger indices for each hour of the 41-year period. A quantile mapping (QM) bias correction technique utilizing available observations during 2003-2012 was used to ameliorate any model biases in wind speed, temperature and relative humidity. Extensive evaluation was undertaken including both quantitative and case study qualitative assessments. The final dataset includes 4-km surface hourly temperature, relative humidity, wind speed, wind direction, Forest Fire Danger Index (FFDI), and daily drought factor (DF) and Keetch-Byram Drought Index (KBDI), and a 32-level full three-dimensional volume atmosphere.

Brown et al. (2015) describes in detail Version 1 of the dataset. This document should be referred to for other details about the project and methods, as well as important caveats when using the dataset.

2 METHODS

Figure 1 shows the process flowchart for creation of the Victoria gridded climatology dataset. The WRF model is initialized with global reanalyses with the primary outputs of surface temperature, relative humidity and wind speed, along with numerous other elements and the full 3-D atmospheric volume. From these data empirical cumulative distribution functions (ECDF) were determined for grid points corresponding to Automatic Weather Station (AWS) hourly observations. ECDFs were also computed for each station. Stricter quality control (QC) methods were applied to the observed data than in the first version. Next, quantile mapping (QM) and bias correction was done for each station location, and spatially interpolated across the grid. All of these steps are described further below.

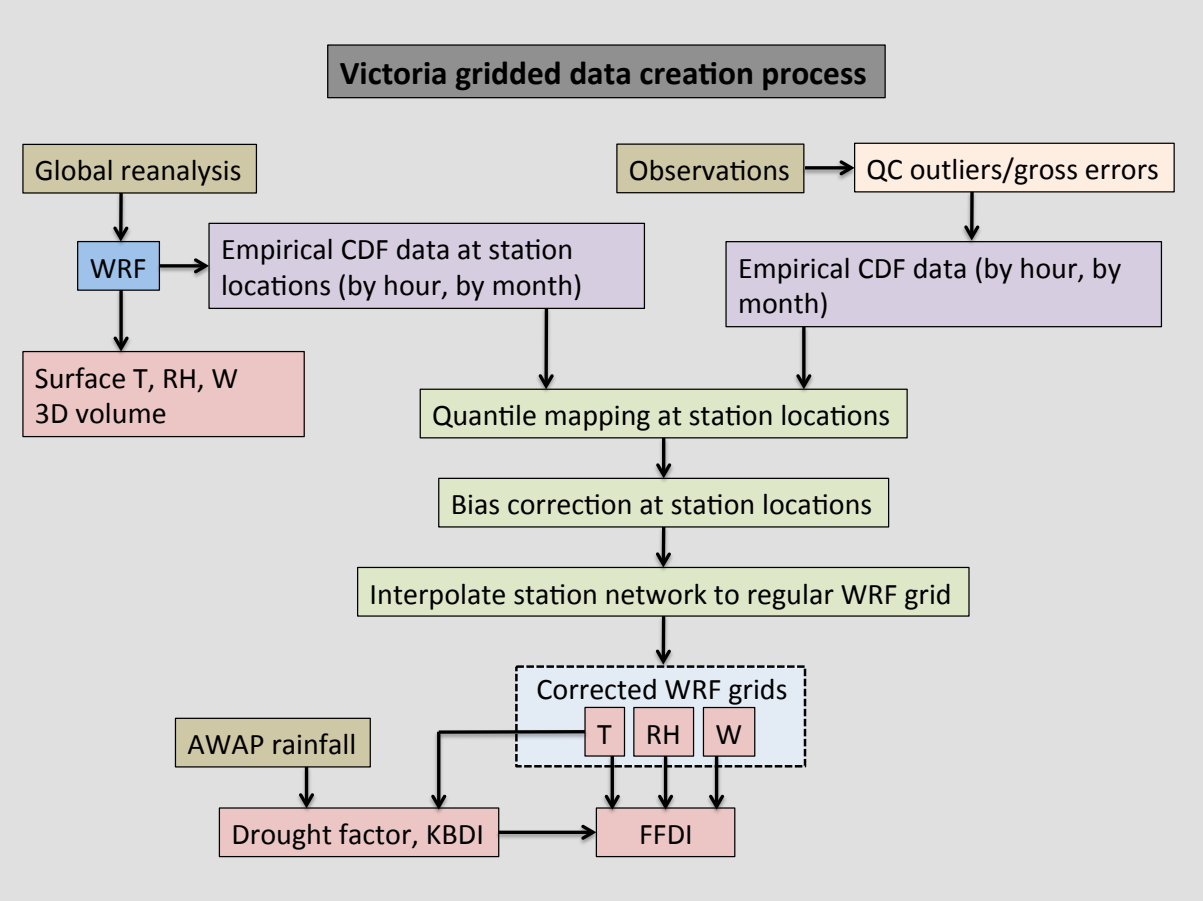

Fig. 1. Process flowchart for creation of the Victoria gridded climatology dataset.

2.1 Bias Correction

A statistical bias (mean error of predicted minus observed) from atmospheric models is not uncommon due to combinations of physics parameterizations, spatial resolution and input data (initial boundary conditions including model type and data assimilation). The bias may run consistently above or below a mean observed value, and thus can be accounted for in the final model output using a statistical correction. However, atmospheric model bias can also be a function of season and hour of the day due to both model physics and the local characteristics of the station siting (e.g., elevation, aspect), requiring a more nuanced statistical correction approach. Figure 2 highlights the diurnal and seasonality of temperature bias (°C) for two Automatic Weather Stations (AWS) in Victoria, Essendon (top) and Bairnsdale (bottom). For Essendon, the overall magnitude of the bias ranges from approximately -0.5 to +2.0°C, though nearly all months and hours have a positive bias. Bairnsdale shows a much greater range of bias from approximately -2.75 to +2.1°C. The seasonality is especially highlighted with a cool bias during the cool season (May-November) for the hours around 0800 through 2100 UTC, which are the local time night and early morning hours. But during the warm season, the highest warm bias is during 0000-0300 hours local time. These examples clearly highlight the need for hourly and seasonal bias correction.

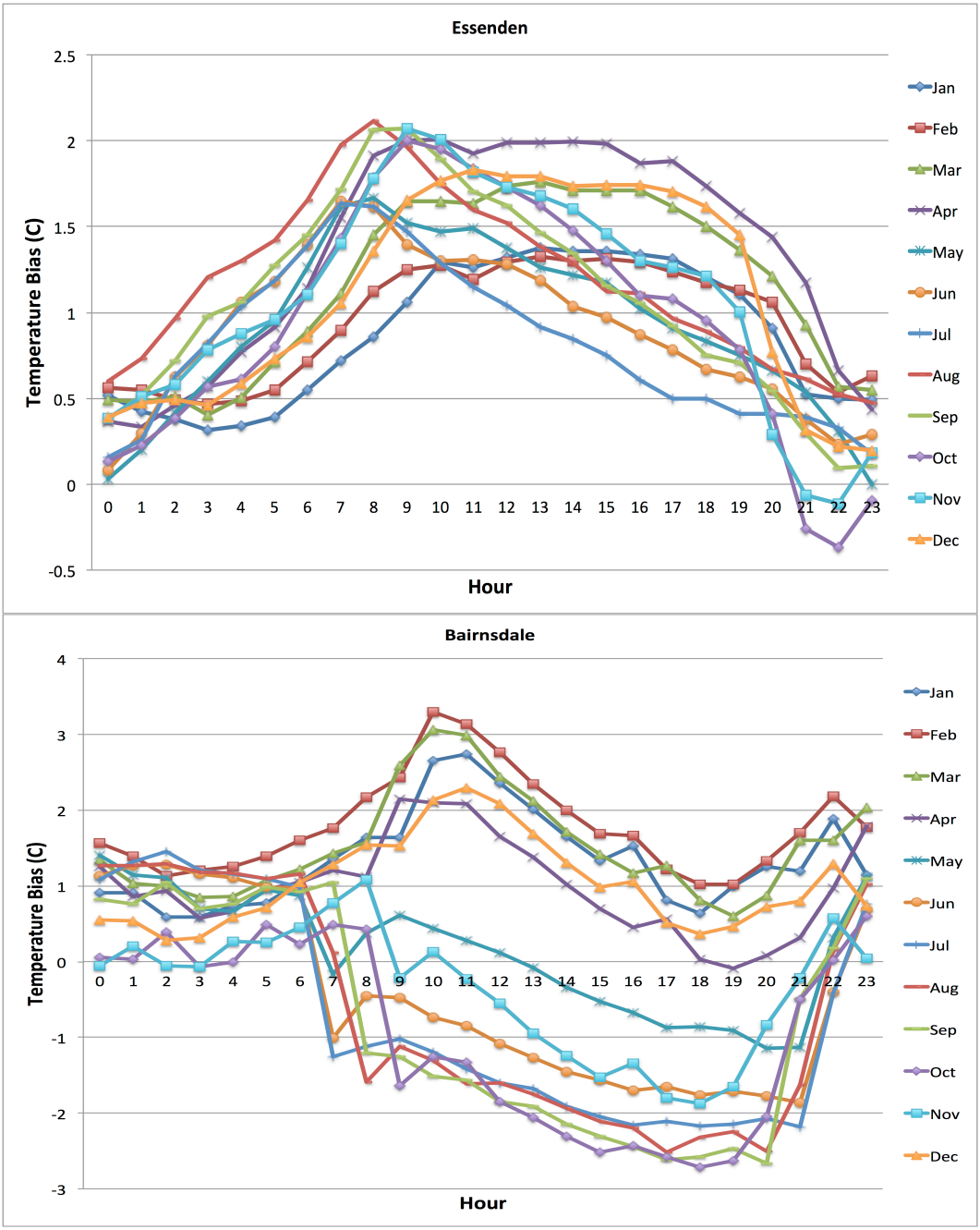

Fig. 2. Hourly (UTC) and monthly temperature bias (°C) for Essendon (top) and Bairnsdale (bottom). The colored symbols and lines correspond to a particular month.

Quantile mapping (QM) for statistical adjustment of bias has been an accepted methodology for many years (e.g., Panofsky and Brier 1968), and has been used for numerous global climate model projection bias corrections (e.g., Maurer et al., 2010, 2014; Thrasher et al., 2012). QM adjusts a model value by mapping quantiles of the model distribution onto quantiles of the observation distribution. Figure 3 provides a visual schematic of the QM process (adapted from Pierce et al., 2015). The blue line shows a hypothetical normal distribution cumulative distribution function (CDF) of observed temperatures and their corresponding quantiles. The red line represents a hypothetical CDF

of model temperatures and their corresponding quantiles. The black horizontal line highlights the 0.2 quantile value. The upward blue dashed line indicates that 10°C is the model 0.2 quantile. The left pointing short arrow shows where the 0.2 quantile intersects the observed temperature value, and the downward pointing arrow shows the observed value that should be used as the bias corrected value. In this case, the WRF 10°C becomes 8.9°C.

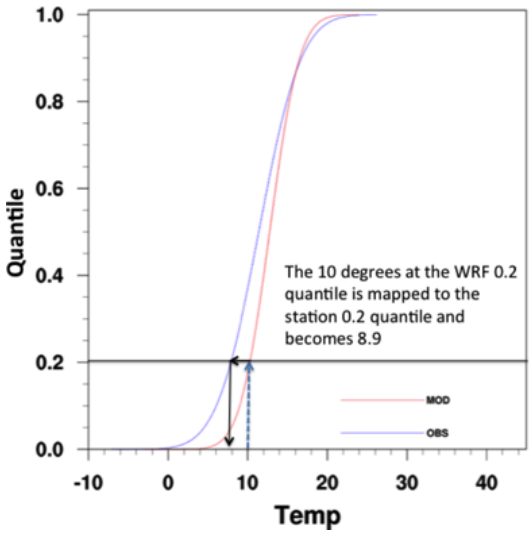

Fig. 3. Example illustrative schematic of the quantile mapping methodology.

Our bias correction process was a multistep approach (Fig. 4). The first step was to gather hourly AWS observations for stations in and bordering Victoria. Data quality control (QC) was applied by first checking for obvious unrealistic values (i.e., negative relative humidity and wind speed; relative humidity > 100%). Next, an exploratory data analysis type check was applied to remove temperature and wind speed outliers that were likely in error. An interquartile range was calculated based on the 20th and 80th percentiles, and multiplied by 3; this value was then added to the 80th percentile number providing a threshold for which any observation exceeding this value was removed. This removed extreme values that were deemed an observation error. Checking of results from this method revealed that indeed questionable values were properly flagged and subsequently removed. As an additional precaution for a temperature check, we checked that no station exceeded the official Bureau of Meteorology maximum and minimum state records. This process yielded maximum and minimum values allowable by hour and month for each station. Only stations that had hourly data for at least 10 years were used yielding 75 stations available for the QM process (Fig. 5). Appendix A provides the list of stations corresponding to the map station index.

Step two was simply to match the AWS location to the nearest WRF land grid point. Testing showed that using water grid points introduced anomalous values in the QM; therefore, it is important to use only land grid points for the cumulative distribution functions.

Step three was the computation of the climatological empirical cumulative distribution functions (ECDF) for each AWS and corresponding matched WRF grid point. Theoretical

distributions (i.e., normal, beta, Weibell for temperature, relative humidity and wind speed, respectively) were originally tested, but it was determined that these did not satisfactorily provide estimates in the distribution tails during the mapping process. ECDFs were determined for each hour for each month (288 functions each for observation and model). For example, if a station had 16 years of hourly data, then an ECDF was computed for hour 00 over all of the 16 years of January. The R software package (R Core Team, 2013) was used to empirically fit the data and determine the quantile values. Figure 6 shows an example ECDF for January 0400 UTC for Melbourne airport. The red (observed) and blue (WRF) curves are for the period 2003-2012. The purple (observed) and yellow (WRF) curves are for the period 1972-2002. Thus, these curves show both the difference between the observed and WRF ECDFs and between the most recent decade versus the previous 31 years. The observed early period is cooler than the recent; this is partially reflected in the higher temperatures for WRF starting around 0.6 quantile.

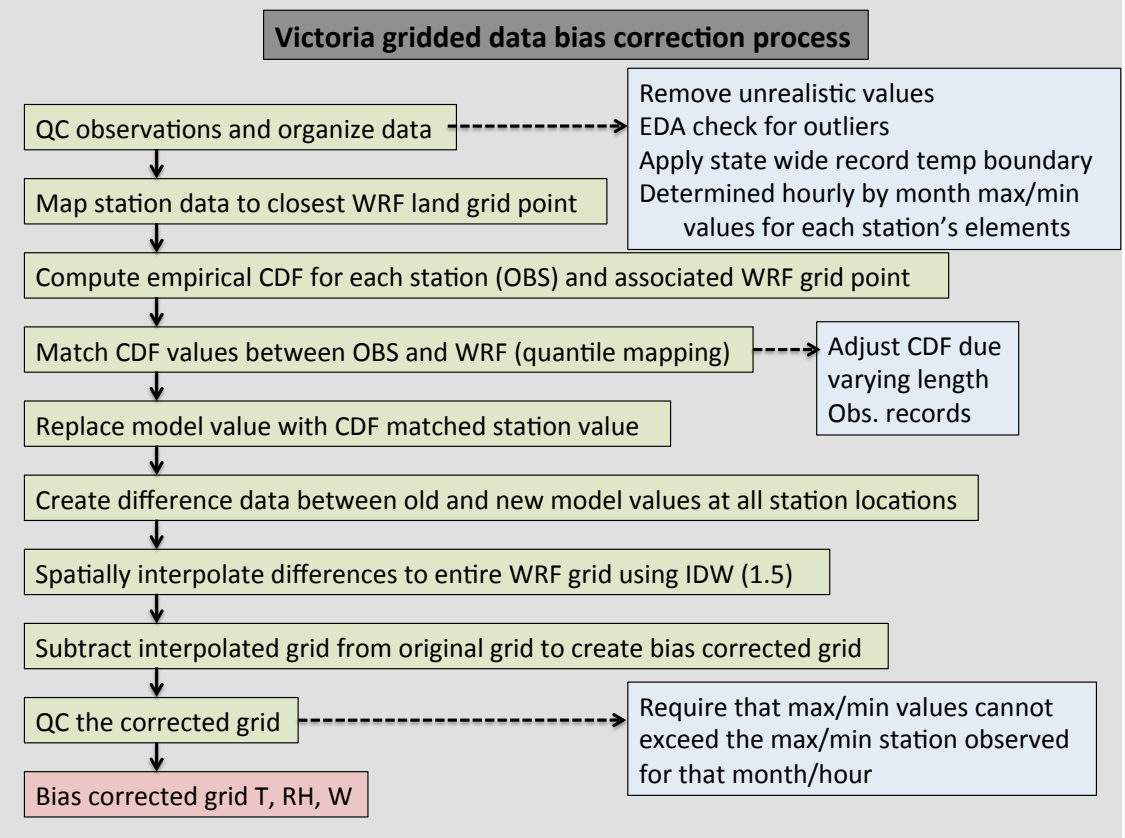

Fig. 4. Flow chart for the bias correction process.

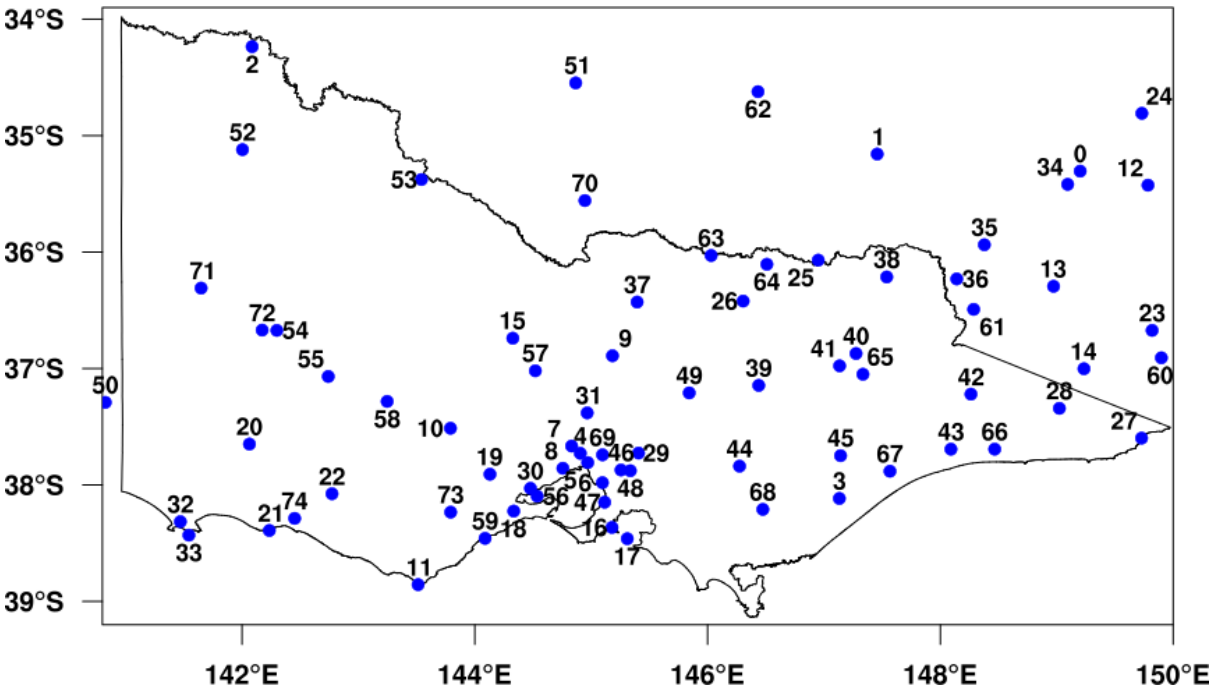

Fig. 5. AWS locations for hourly stations used in the development of the quantile mapping for bias correction. The numbers indicate a station index (see Brown et al., (2016) for station information). Appendix A provides the list of stations corresponding to the map station index.

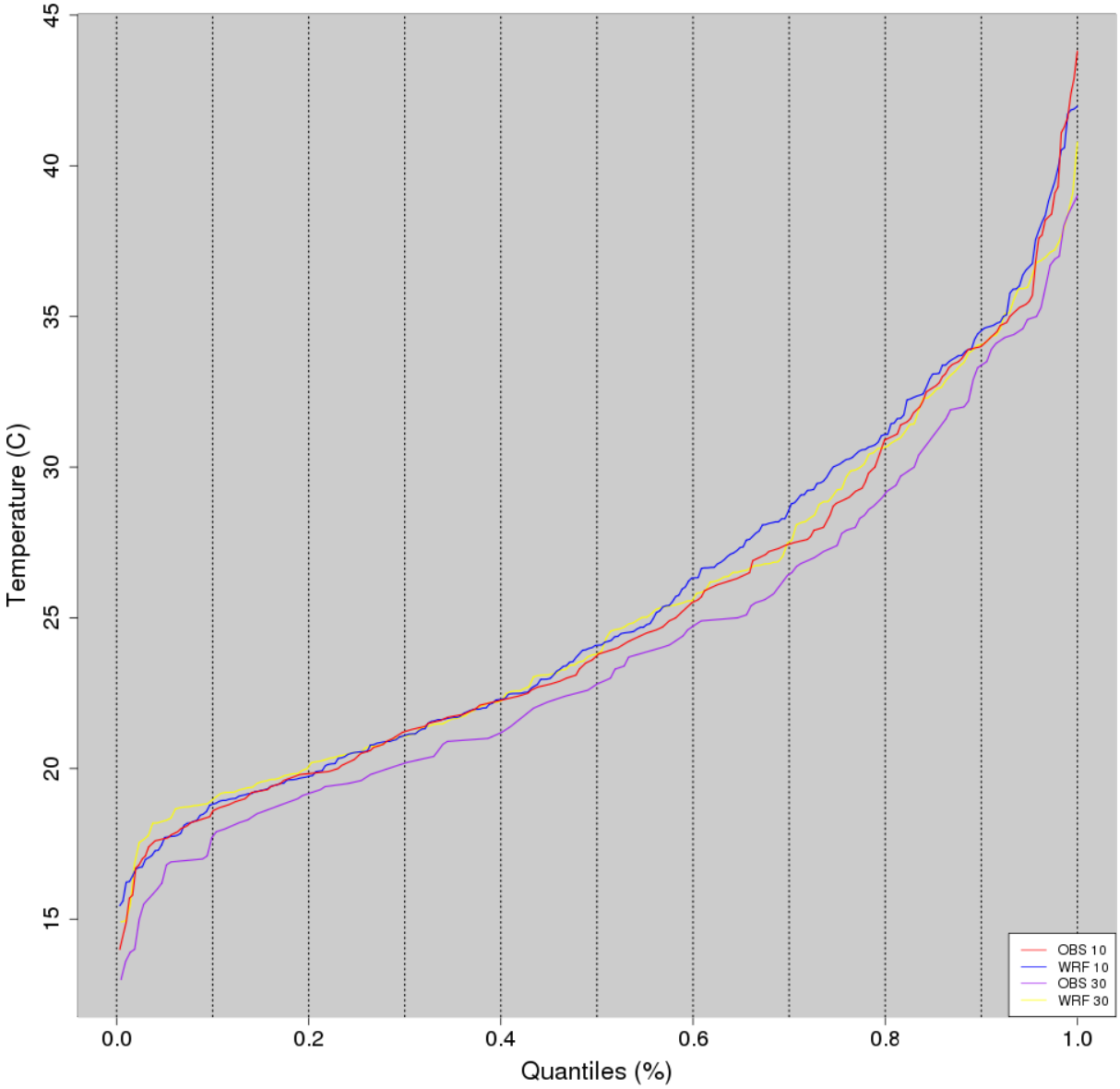

Fig 6. Example empirical cumulative distribution function for Melbourne airport January 0400 UTC. The red (observed) and blue (WRF) curves are for the period 2003-2012. The purple (observed) and yellow (WRF) curves are for the period 1972-2002.

The next steps are the actual bias correction. Each of these steps was applied to all available hours of station data. In step 5, the model value was replaced with the ECDF matched station value per the process described for Figure 4. This step created new model values for each station location. Step 6 created a difference dataset between the old and new model values at all station locations. This allowed for spatially interpolating a difference field across the 4-km grid (step 7). The "dsgrid2" inverse distance weighting spatial interpolation algorithm with a power coefficient of 1.5 in the NCAR Command Language (NCL, 2012) software package Inverse distance weighting (IDW) was used for the spatial interpolation method. The power coefficient of 1.5 was subjectively chosen based upon examining output maps. It was felt that 1.5 allowed for reasonable weighting of nearby stations, but still retained sufficient local information. Higher power coefficient values localize the weighting, while lower values distribute station influence more widely. Step 8 simply subtracted the

interpolated grid from the original grid to create the bias corrected grid for that hour. Figure 7 shows example maps of two difference grids representing hours 0500 and 1700 local time for 7 February 2009. Note in this example that the early morning hour of 0500 requires greater corrections especially in the complex terrain region than for the late afternoon hour of 1700. This is primarily due to the model's nighttime physics and the local topographic influences of complex terrain.

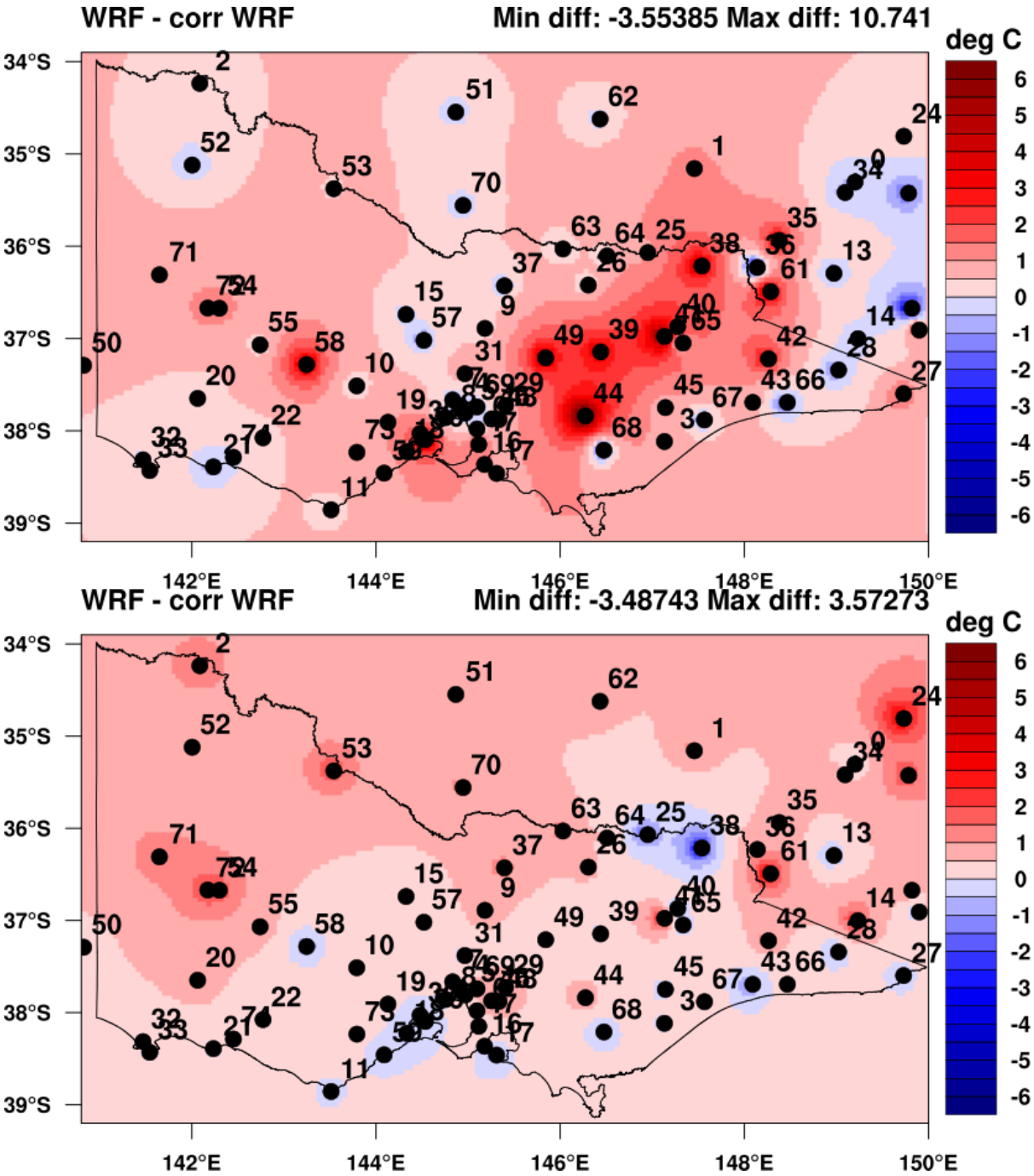

Fig. 7. Spatial interpolation examples from the quantile mapping bias correction for 7 February 2009 0500 local time (top) and 1700 local time (bottom). Shaded values are WRF uncorrected grid point values minus WRF bias corrected grid point values for temperature (°C).

The final step in the process was a check of the final grid requiring that the maximum/minimum values of the new grid did not exceed the maximum/minimum values of station observed values. This step kept the bias corrected values as estimates across the grid from exceeding the known observed values. It certainly is possible that locations in between stations could achieve observed values exceeding observed, but given there are not observations everywhere, it was felt that this conservative approach still allowed for realistic climatological representations while keeping the model values within ranges known measurements.

The results of the bias correction can be partially assessed by examining example station boxplots and scatterplots. Figure 8 (top) shows an example for the January 2003-2012 hourly (UTC) distribution of WRF minus observed temperature (°C) for the Melbourne airport station before bias correction. Overall, the bias is quite low (approximately ±0.5°C. The outlying points are due to likely due to a timing issue of fronts and other localized circulation patterns or phenomena that WRF missed, and these cannot be corrected for strictly from the bias correction process. The bottom plot of Fig. 8 shows the distribution after the bias correction. Though not all medians fall on the zero line, the interquartile distribution is more centered around zero degrees. The majority of the outliers are WRF over-predicting temperature.

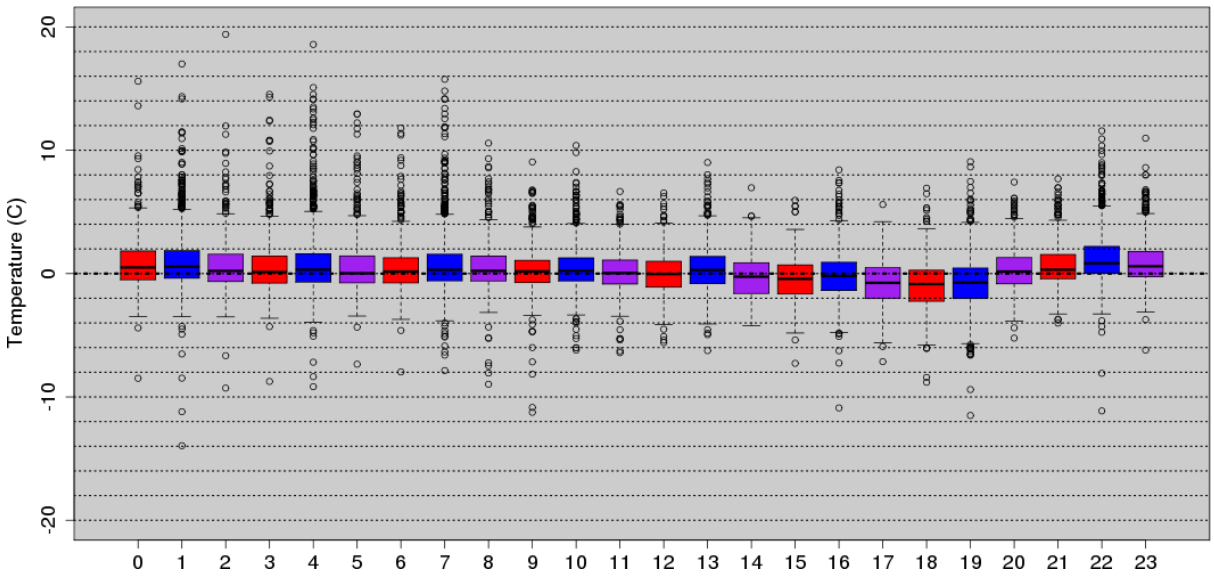

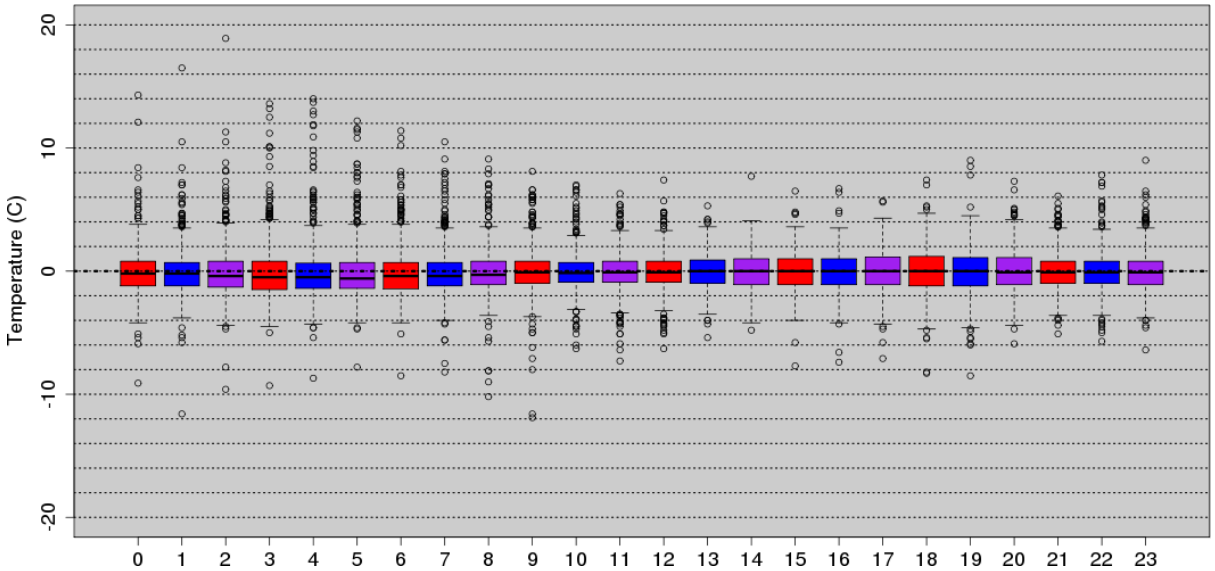

Fig. 8. Boxplots of January 2003-2012 hourly (UTC) distribution of WRF minus observed temperature (°C) for Melbourne airport before bias correction (top) and WRF bias corrected minus observed (bottom).

Figure 9 (top) shows the original bias for Melbourne airport 2003-2012 January relative humidity (%). The median bias is generally small, with the exception hours 15-19 UTC, which are early morning hours in local time. The bias corrected values are also shown in Fig. 9 (bottom), and show good centering of the interquartile range around zero with median values of 0-1%. Similar to temperature, there are some outliers from frontal timing, local precipitation events, or other factors for which the correction method cannot adjust. The majority of these outliers are WRF under-predicting relative humidity.

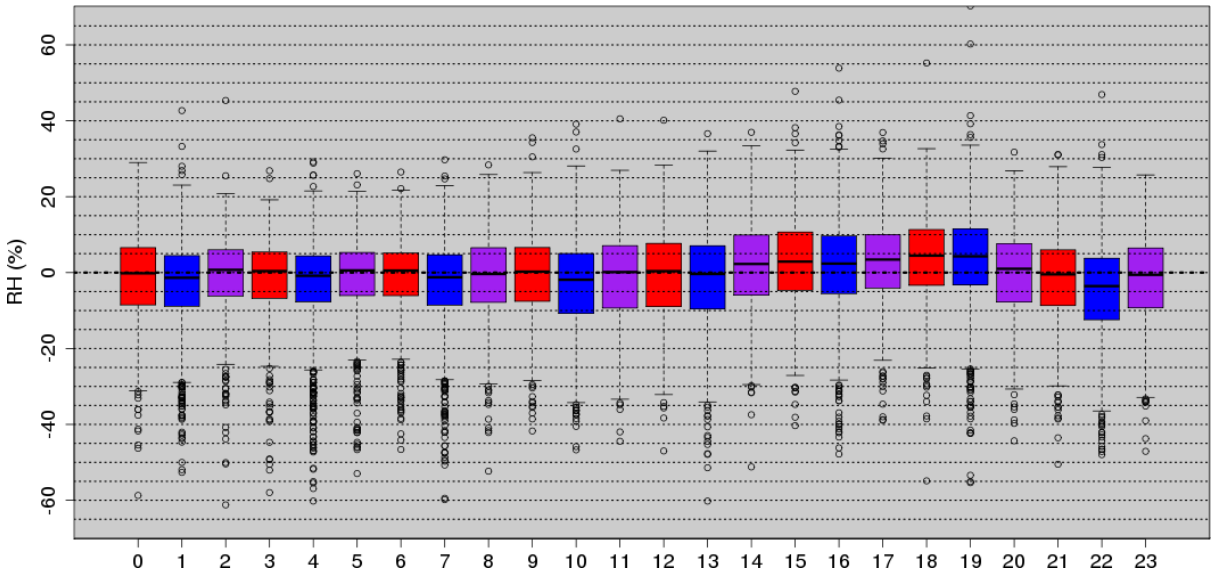

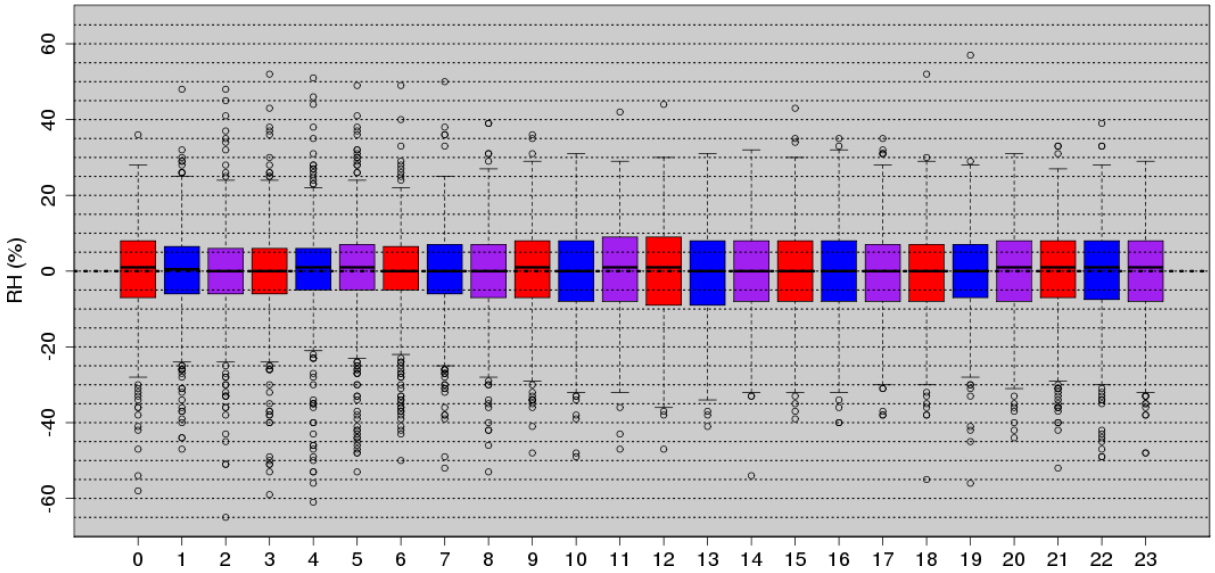

Fig. 9. Boxplots of January 2003-2012 hourly (UTC) distribution of WRF minus observed relative humidity (%) for Melbourne airport before bias correction (top) and WRF bias corrected minus observed (bottom).

Figure 10 (top) shows the original bias for Melbourne airport 2003-2012 January wind speed (knots). The median original bias is in the 0-2 knot range, though overall WRF tended to under-predict wind speed. Similar to Figs. 8 and 9, there are outliers related to other model and observation factors beyond just bias. Figure 10 (bottom) shows overall improvement from the bias correction. Though there is still a slight under-prediction, the median values are now 0-1 knots, and the overall distribution is more condensed.

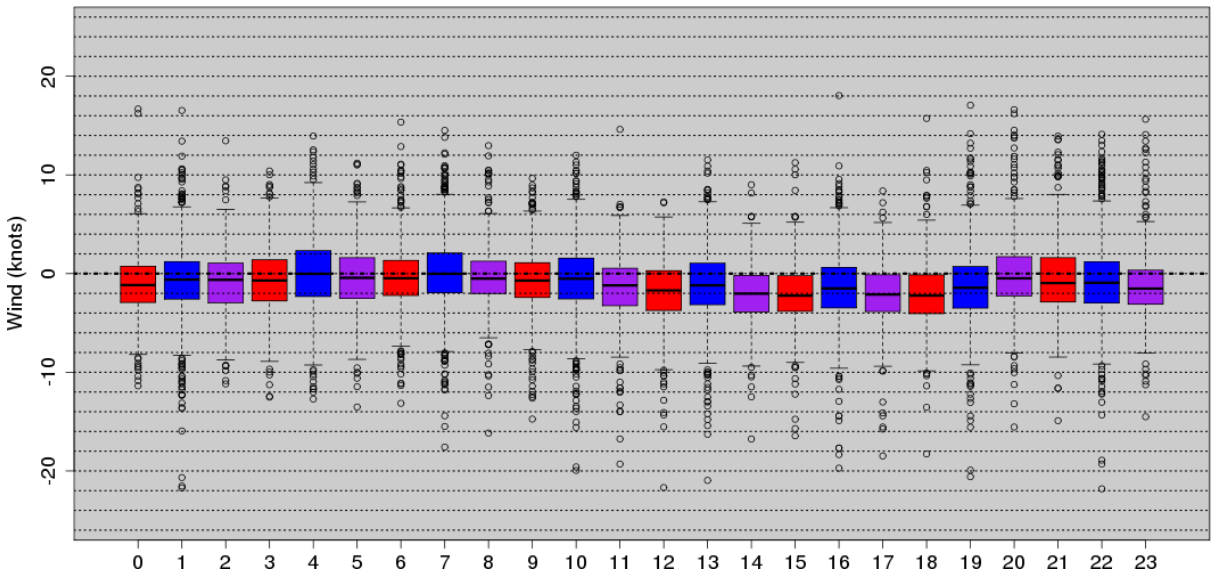

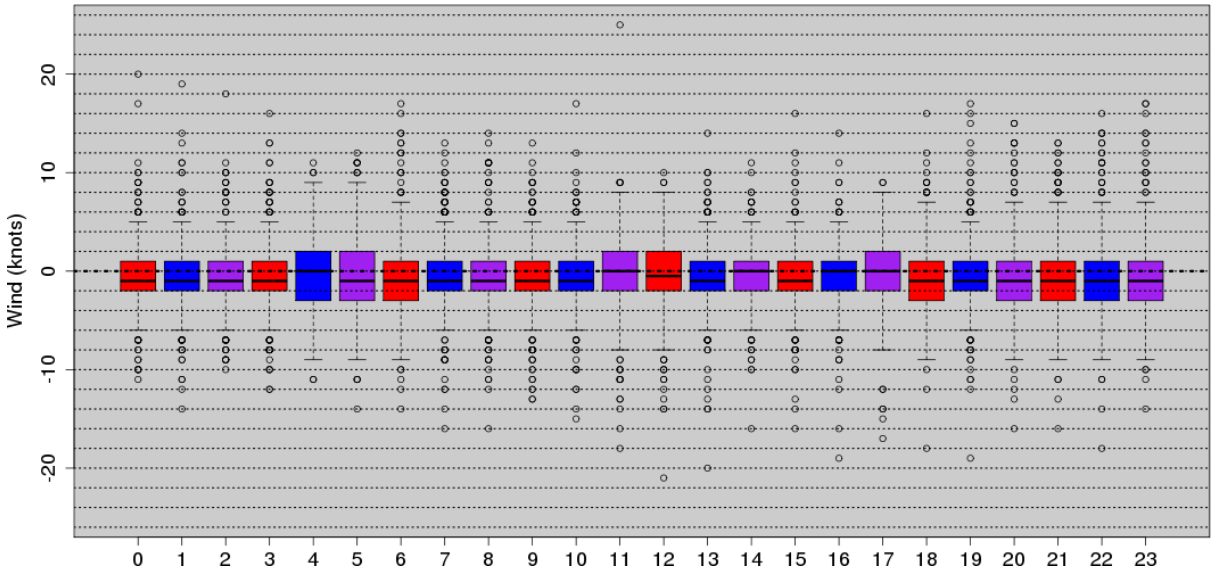

Fig. 10. Boxplots of January 2003-2012 hourly (UTC) distribution of WRF minus observed wind speed (knots) for Melbourne airport before bias correction (top) and WRF bias corrected minus observed (bottom).

Figure 11 shows example scatterplots for WRF predicted versus observed temperature for January 0000 UTC. The blue circles show before and the red circles after QM bias correction, respectively. Figure 11 (top) is for Falls Creek where both scatterplots show a well-defined linear relationship, but the before correction scatter clearly highlights WRF over-predicting temperature. The QM bias correction shows the values nicely aligned along the 45° diagonal. As shown in the previous boxplot examples, there remain some points in which the errors could not be substantially reduced. Figure 11 (middle) shows January 0000 UTC scatterplots for Horsham Aerodome. In this case there is little difference between the predicted versus observed points before and after correction, indicating that little QM correction was needed to begin with. As a final example, Fig. 11 (bottom) shows January 0000 UTC scatterplots for Mount Hotham, where there was a clear need for bias correction, and several points show large errors between predicted and observed. Many of these larger errors were reduced after correction, and generally the points align better along the diagonal.

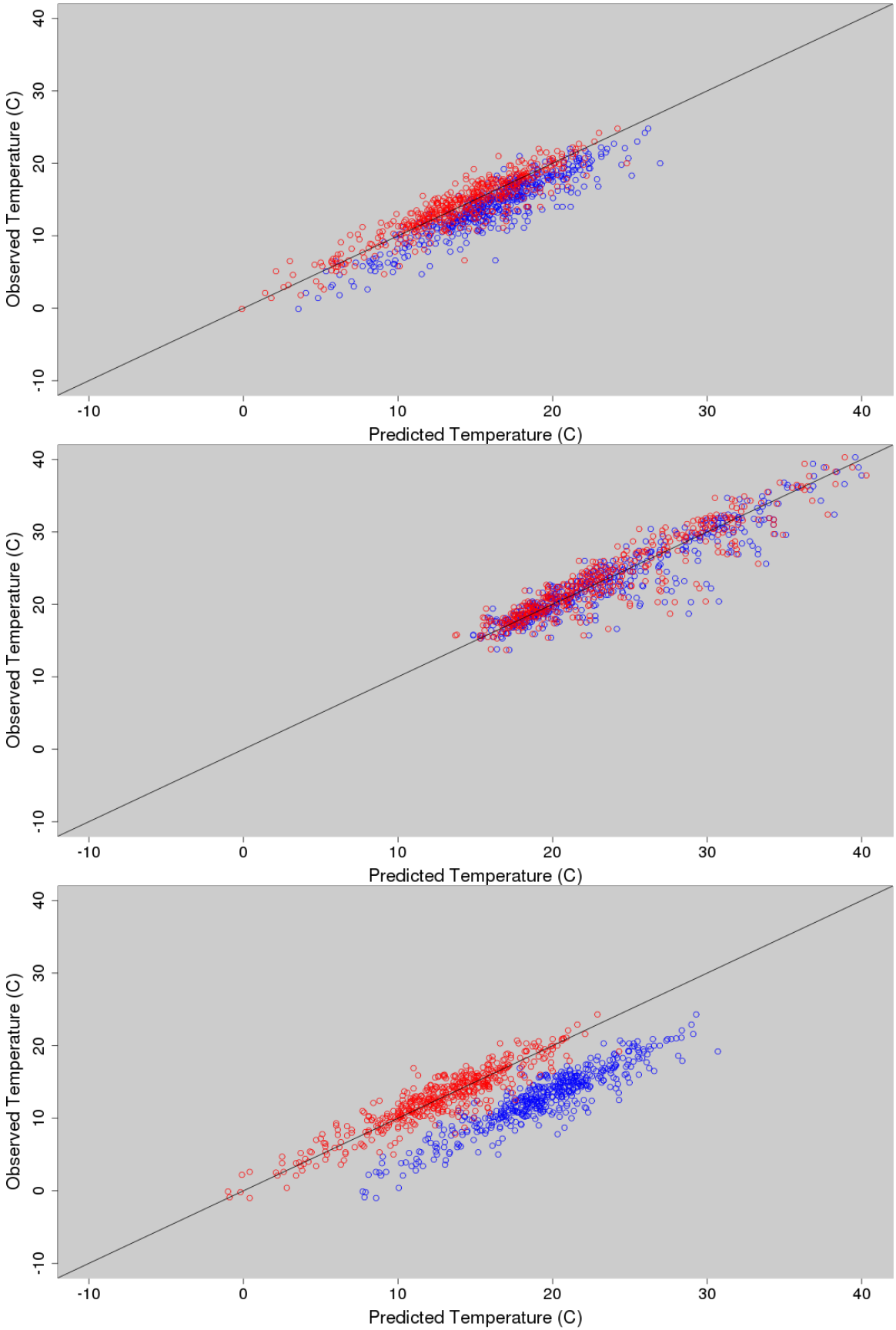

Fig. 11. Scatterplots of WRF predicted versus observed temperature (°C) for January hour 0000 UTC for the years 2003-2012 for the stations Falls Creek (top), Horsham Aerodome

(middle), and Mount Hotham (bottom). Blue and red circles are before and after, respectively, bias correction.

3 RESULTS

3.1 VERSION 2 OF THE DATA SET

This version of the dataset includes hourly temperature, relative humidity, wind speed, wind direction, and FFDI, and daily DF and KBDI at a 4-km spatial resolution for the period 1972-2012. The bias correction method described in Section 2.1 above was applied to temperature, relative humidity, and wind speed. Because of quality issues with precipitation discussed Brown et al. (2015), AWAP data were used instead to calculate daily DF and KBDI and then these were used (in combination with bias corrected hourly temperature, relative humidity, and wind speed) to calculate hourly FFDI.

3.2 CLIMATOLOGY

Numerous climatology analyses can be undertaken with this dataset, both for diagnostic and summary assessments. Here we show a few examples.

The homogeneous 4 km grid in the dataset allows for a variety of annual, seasonal, monthly, daily, and hourly spatial analyses. Figure 12 shows the average January temperature for 0600 UTC (upper left) and 1800 UTC (lower left), and corresponding relative humidity in the upper right and lower right, respectively. These times represent approximately the daily maximum and minimum values of the diurnal cycle during January. There is a clear diurnal cycle, with the topography modifying the absolute values of temperature, and a strong modification of the airmass south of the ranges by the effects of land-sea contrast. The relative humidity distribution and diurnal variation approximately follows the temperature distribution due to the negative relationship of relative humidity with temperature, but the effects of topography are somewhat different, probably due to the normal hydrolapse.

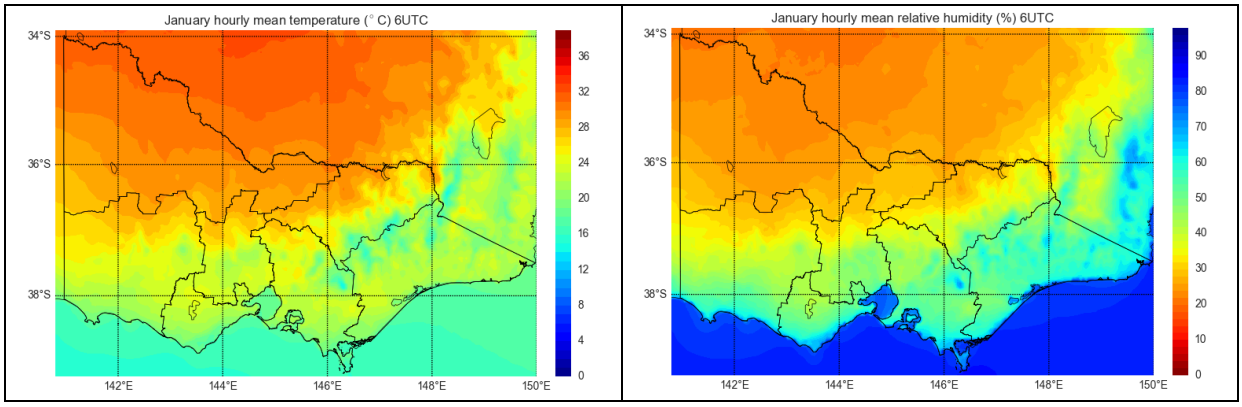

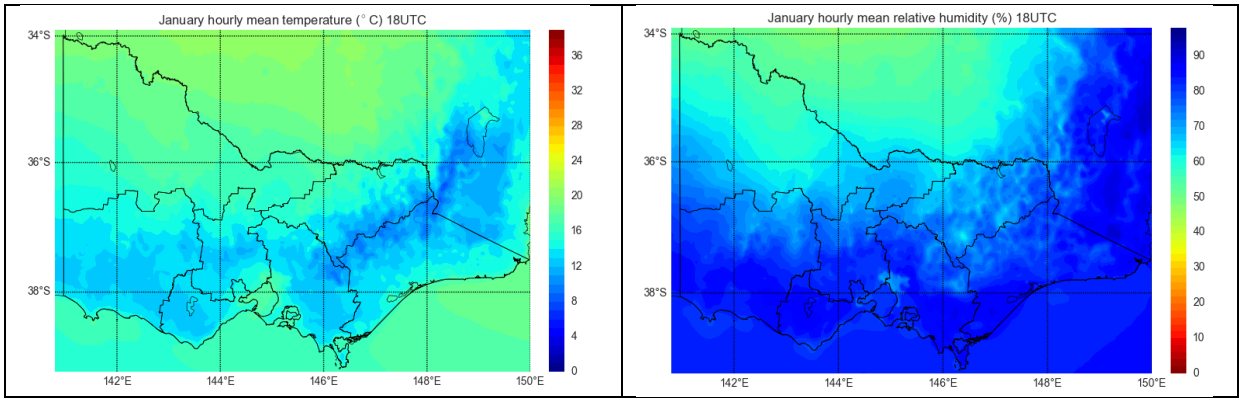

Fig. 12. Average January temperature and relative humidity for hour 0600 UTC (top left and right) and hour 1800 UTC (bottom left and right). The geographic boundaries represent Bushfire Risk landscape boundaries used by DELWP.

Figure 13 shows December-February all-time maximum temperature (left map) and minimum relative humidity (right map) for the years 1972-2012. The highest temperatures are seen in the northwest portion of the state, and the coolest in the higher elevations of the Great Dividing Range in the East, and shows the sharp temperature contrast along the coast. For most of Victoria, the all-time lowest humidity values are below 15%. It is interesting that there is less variation across the state in these extreme values than there is in the average 0600 UTC (January) fields shown in Fig. 12, indicating that even in the relatively benign climates, such as that of east Gippsland, very high temperatures and very low relative humidities can occur.

Comparing Fig. 13 with the equivalent geographical distributions for version 1 of the data set (Fig.33 of Brown et al 2015) shows relatively subtle differences for the temperatures, but in Version 2, the lowest relative humidity is lower over almost the whole state than was that of Version 1. This indicates the reduction in moist bias seen at the lowest relative humidity values in Version 1.

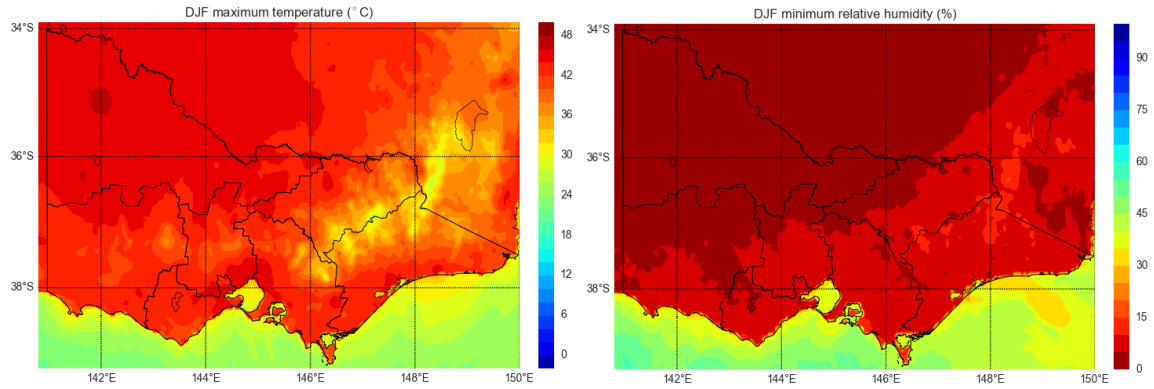

Fig. 13. December-February all-time maximum temperature (left map) and minimum relative humidity (right map) for the years 1972-2012.

Figure 14 shows the 1972-2012 December-February maximum FFDI at each gridpoint.. There is some small-scale variability in the northwest, and understanding this requires further investigation, but it appears to be associated with very isolated high wind speeds in the WRF data set, together with the extreme sensitivity of the FFDI to variations in its inputs when the values reach high levels. On a broader scale, the highest FFDI values are seen in the northwestern portion of Victoria, extending eastwards to central Victoria north of the ranges, and southwards in the far west of the state. There are also notable areas of high values south of the central highlands just west of Melbourne and extending westward along the Barwon Valley, and also areas of relative maximum in west and central Gippsland – both these areas appear associated with lee effects of the ranges. The lowest values are seen across the Great Dividing Range in the east where elevation effects keep temperatures lower, and in far-east Gippsland.

Comparing these values with those from Version 1 of the data set (Fig. 34 of Brown et al 2015) shows similar patterns, but with generally higher values, in Version 2 (note the differing data ranges in the two figures). This is the effect of the new QM better representing the high wind speed and low relative humidity tails of the respective distributions, with consequent effects on the resulting FFDI values. There are also some differences between the patterns along the coastline, where greater attention to station-gridpoint interpolation issues has led to changes that provide a more realistic representation.

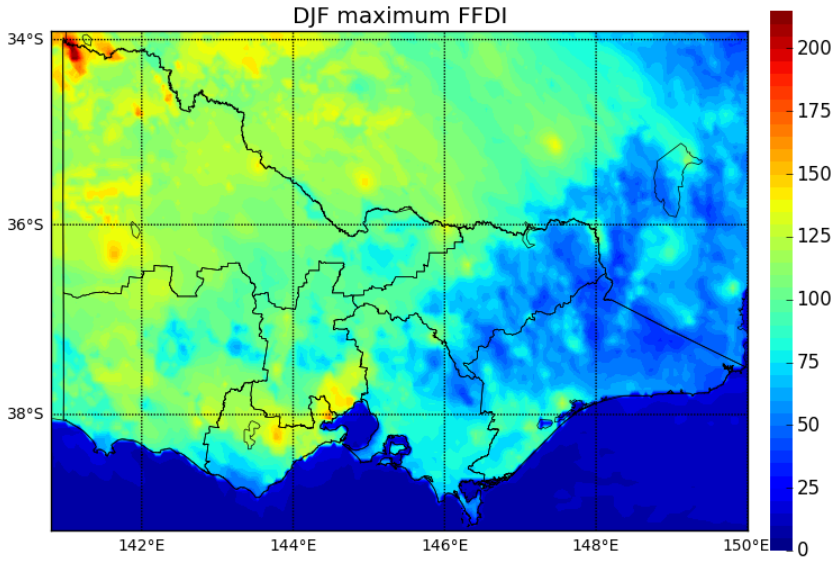

Fig. 14. December-February highest value of FFDI for the years 1972-2012 from the gridded climatology.

4 SUMMARY AND CONCLUSION

Version 2 of the dataset is substantially improved over Version 1, and thus replaces Version 1. The improvements were due to stricter QC and thresholds in the observational data, and applying empirical cumulative distribution functions for the quantile mapping. This allowed for improved bias correction in the tails of the distribution, and thus have better

represented extremes in both the individual parameters and also in the derived FFDI values. This is important for fire analyses since it is extreme fire events that are often of most interest.

5 DATA STORAGE AND ACCESS

At the time of writing this report, the complete dataset is stored at Monash University with a backup and at DRI. Two file groups are available, the original uncorrected fields for all levels, and bias corrected surface fields based on the quantile mapping method described in this report. The file format is netCDF, which contains relevant metadata as part of the data structure.

Derived fields include the Drought Factor (DF), Keetch-Byram Drought Index (KBDI), and Forest Fire Danger Index (FFDI). Daily precipitation from the Australian Water Availability Project (AWAP) dataset was used for the DF and KBDI calculations. FFDI was calculated using these outputs along with temperature, relative humidity and wind speed from the WRF dataset. These derived fields are also in the netCDF format.

The full dataset (including the upper-air fields) is approximately 53TB in size. The surface fields commonly used for bushfire analyses (e.g., temperature, relative humidity and wind speed) are much smaller, and formatted in netCDF allowing for direct input into Phoenix. Metadata description for the dataset is available upon request.

Questions and comments regarding the dataset may be directed to:
Dr. Tim Brown; tim.brown@dri.edu, or
Dr. Sarah Harris; sarah.harris@monash.edu

6 ACKNOWLEDGEMENTS

This project would not have been possible without the support and encouragement from Liam Fogarty at the Department of Environment, Water, Land and Planning (DEWLP) and Alen Slijepcevic (Country Fire Authority; formerly DEWLP). We very much appreciate Andy Ackland at DEWLP for testing output data in Phoenix. This work was funded under the Victoria Department of Sustainability and Environment Project 92c – Weather Research Forecasting Model – Victoria Fire Climatology Gridded Dataset.

7 REFERENCES

Brown, T., G. Mills, S. Harris, D. Podnar, H. Reinbold, and M. Fearon, 2015: Fire Weather Climatolology Dataset for Victoria. Final Project Report to the Victoria Department of Environment, Land and Water Planning, August 2015, 134 pp.

8 APPENDICES

Appendix A: Table of AWS stations and years used in the bias correction analysis.

Map ID	Station name	Station ID	Start year	End year	# of years
0	CANBERRA AIRPORT	70014	1996	2010	15.0
1	WAGGA WAGGA AMO	72150	1996	2013	17.3
2	MILDURA AIRPORT	76031	1996	2013	17.5
3	EAST SALE AIRPORT	85072	1996	2013	16.7
4	ESSENDON AIRPORT	86038	2003	2013	10.5
5	MELBOURNE REGIONAL OFFICE	86071	1997	2013	13.2
6	MOORABBIN AIRPORT	86077	1996	2013	17.3
7	MELBOURNE AIRPORT	86282	1996	2013	17.6
8	LAVERTON RAAF	87031	1996	2013	16.9
9	MANGALORE AIRPORT	88109	1996	2013	17.0
10	BALLARAT AERODROME	89002	2000	2013	12.9
11	CAPE OTWAY LIGHTHOUSE	90015	1996	2013	17.2
12	BRAIDWOOD RACECOURSE AWS	69132	1996	2013	17.0
13	COOMA AIRPORT AWS	70217	1996	2013	17.2
14	BOMBALA AWS	70328	1996	2013	16.9
15	BENDIGO AIRPORT	81123	1996	2013	16.9
16	CERBERUS	86361	1996	2013	15.5
17	RHYLL	86373	1996	2013	17.2
18	GROVEDALE (GEELONG AIRPORT)	87163	1996	2011	15.6
19	SHEOAKS	87168	1996	2013	16.7
20	HAMILTON AIRPORT	90173	1996	2013	16.5
21	PORT FAIRY AWS	90175	1996	2013	17.3
22	MORTLAKE RACECOURSE	90176	1996	2013	16.7
23	BEGA AWS	69139	1996	2013	16.7
24	GOULBURN AIRPORT AWS	70330	1996	2013	17.0
25	ALBURY AIRPORT AWS	72160	1996	2013	17.1
26	WANGARATTA AERO	82138	1996	2013	17.0
27	MALLACOOTA	84084	1996	2013	16.7
28	COMBIENBAR AWS	84143	1996	2013	16.9
29	COLDSTREAM	86383	1996	2013	17.1
30	AVALON AIRPORT	87113	1996	2013	16.9
31	WALLAN (KILMORE GAP)	88162	1996	2013	15.4
32	PORTLAND (CASHMORE AIRPORT)	90171	1996	2013	16.9
33	CAPE NELSON LIGHTHOUSE	90184	1997	2013	16.1
34	TUGGERANONG (ISABELLA PLAINS) AWS	70339	1996	2013	16.9
35	CABRAMURRA SMHEA AWS	72161	1996	2013	16.0

36	KHANCOBAN AWS	72162	1996	2013	15.9
37	SHEPPARTON AIRPORT	81125	1996	2013	16.8
38	HUNTERS HILL	82139	1996	2013	17.0
39	MOUNT BULLER	83024	1996	2013	14.0
40	FALLS CREEK	83084	1996	2013	16.6
41	MOUNT HOTHAM	83085	1996	2013	16.0
42	GELANTIPY	84142	1996	2013	17.1
43	MOUNT NOWA NOWA	84144	1996	2013	17.3
44	MOUNT BAW BAW	85291	1996	2013	14.2
45	MOUNT MOORNAPA	85296	1996	2013	17.0
46	SCORESBY RESEARCH INSTITUTE	86104	1996	2013	16.6
47	FRANKSTON AWS	86371	1996	2013	17.3
48	FERNY CREEK (DUNNS HILL)	86372	1996	2011	15.5
49	EILDON FIRE TOWER	88164	1996	2013	17.1
50	COONAWARRA	26091	1997	2013	14.9
51	HAY CSIRO AWS	75175	1996	2007	10.1
52	WALPEUP RESEARCH	76064	1998	2013	14.5
53	SWAN HILL AERODROME	77094	1997	2013	15.9
54	LONGERENONG	79028	1997	2013	16.0
55	STAWELL AERODROME	79105	1996	2013	17.2
56	POINT WILSON	87166	1996	2008	11.6
57	REDESDALE	88051	1997	2013	14.4
58	LOOKOUT HILL	89105	1996	2007	10.9
59	AIREYS INLET	90180	1996	2013	17.3
60	MERIMBULA AIRPORT AWS	69147	1998	2013	14.9
61	THREDBO AWS	71032	1998	2013	14.8
62	YANCO AGRICULTURAL INSTITUTE	74037	1999	2013	13.4
63	YARRAWONGA	81124	2002	2013	11.0
64	RUTHERGLEN RESEARCH	82039	1998	2013	15.1
65	DINNER PLAIN (MOUNT HOTHAM AIRPORT)	83055	2000	2013	12.8
66	ORBOST	84145	2000	2013	12.6
67	BAIRNSDALE AIRPORT	85279	1997	2013	15.2
68	MORWELL (LATROBE VALLEY AIRPORT)	85280	1997	2013	16.0
69	VIEWBANK (ARPANSA)	86068	2000	2013	13.0
70	DENILIQUIN AIRPORT AWS	74258	1997	2013	16.0
71	NHILL AERODROME	78015	2003	2013	10.1
72	HORSHAM AERODROME	79100	1997	2013	15.3
73	COLAC (MOUNT GELLIBRAND)	90035	2000	2013	12.8
74	WARRNAMBOOL AIRPORT NDB	90186	1998	2013	14.9

Appendix B. Dataset description: Fire Weather Climatology for Victoria

Readme version date: 22 June 2016

Dataset version “June 2016”.

This dataset replaces Version 1. Substantial improvements to the dataset were made, especially in the distribution tails due to 1) modifications of the quantile mapping bias correction method, and 2) additional quality control checking on the surface station observations used for the bias correction.

This dataset includes the surface elements produced from the Fire Weather Climatology for Victoria project documented in the report by Brown et al (2015; 2016). Please see that report for the details of the construction and applicability of these data.

The dataset period is January 1972 – December 2012.

Produced using model version “WRF v3.5.1”

The temporal scale is hourly.

The horizontal resolution is 4x4 km.

Two file groups are available, original uncorrected fields and bias corrected fields based on the quantile mapping method described in the report.

The file format is netCDF, which contains relevant metadata as part of the data structure.

Derived fields include the Drought Factor (DF), Keetch-Byram Drought Index (KBDI), and Forest Fire Danger Index (FFDI). Daily precipitation from the Australian Water Availability Project (AWAP) dataset was used for the DF and KBDI calculations. FFDI was calculated using these outputs along with temperature, relative humidity and wind speed from the WRF dataset. These derived fields are also in the netCDF format.

The dataset was constructed primarily for climatological analyses; hourly data should be examined carefully for specific case study analyses.

WRF surface output in this dataset:

Variable = Temperature (T)
FillValue = -32767.0
projectionType = "MERCATOR"
level = "SFC"
units = "C"
gridType = "SCALAR"
lonCentre = 145.4

Variable = Relative Humidity (RH)
FillValue = -32767.0
projectionType = "MERCATOR"
level = "SFC"
units = "%"
gridType = "SCALAR"
lonCentre = 145.4

Variable = Wind speed (WSPD)
FillValue = -127.0
projectionType = "MERCATOR"
level = "SFC"
units = "kts"
gridType = "VECTOR"
lonCentre = 145.4

Variable = Wind direction (WDIR)
FillValue = -127.0
projectionType = "MERCATOR"
level = "SFC"
units = "degrees"
gridType = "VECTOR"
lonCentre = 145.4

Variable = Precipitation (PPT)
FillValue = -32767.0
projectionType = "MERCATOR"
level = "SFC"
units = "mm"
gridType = "SCALAR"
lonCentre = 135.0

When using these data, please cite the Brown et al (2015; 2016):

Brown, T., G Mills, S. Harris, D. Podnar, H. Reinbold, and M. Fearon, 2015: Fire weather climatology data for Victoria. Final project report, July 2015.

Brown, T., G Mills, S. Harris, D. Podnar, H. Reinbold, and M. Fearon, 2016: Fire weather climatology data for Victoria. Supplemental report for Dataset Version 2, June 2016.

For questions or comments, please contact:

Tim Brown, tim.brown@dri.edu
Or
Sarah Harris, sarah.harris@monash.edu